Available online at www.sciencedirect.com
ScienceDirect
Acta Materialia 57 (2009) 2896–2908
Acta MATERIALIA
www.elsevier.com/locate/actamat

An assessment of the entire Al–Fe system including $D0_3$ ordering

Bo Sundman [a,*], Ikuo Ohnuma [b], Nathalie Dupin [c], Ursula R. Kattner [d], Suzana G. Fries [e,f]

[a] CIRIMAT, UPS/CNRS/ENSIACET, 116 Route de Narbonne, 31077 Toulouse, France
[b] Department of Materials Science, Tohoku University, Sendai, Japan
[c] Calcul Thermodynamique, FR 63670 Orcet, France
[d] National Institute of Standards and Technology, Gaithersburg, MD, USA
[e] SGF Scientific Consultancy, Aachen, Germany
[f] ICAMS, Ruhr University Bochum, Bochum, Germany

Received 10 December 2008; received in revised form 15 December 2008; accepted 27 February 2009
Available online 9 April 2009

Abstract

The Al–Fe system is important for many alloys and the new interest in iron aluminides makes it necessary to improve the modeling of the different ordered forms on the body-centered cubic lattice in this system. This has now been done using a four-sublattice model based on the compound energy formalism, which can describe disordered A2 and the B2, $D0_3$ and B32 ordering. The chemical and ferromagnetic ordering transitions can be both first and second-order and they have a strong interaction. Almost all available experimental and theoretical data for all phases in the system have been fitted within estimated uncertainties.

Keywords: Calphad; Ordering; Compound energy formalism; Phase diagram; Al–Fe

1. Introduction

Many assessments of important binary systems still used in commercial databases were typically derived 10–15 years ago, when the computer facilities were new for most researchers in materials science. The thermodynamic descriptions of many of these systems have often been amended, sometimes without proper publication. New experimental data and *ab initio* calculations, especially for metastable states, have also been published and the modeling technique has improved, which makes it important to present a complete review of many of these binary systems. This has to be done even if it is not possible to integrate these new assessments directly into existing commercial databases because all higher-order systems which have been assessed using the previous assessment will also have to be revised.

The emphasis of this paper is on modeling issues; the evaluation of the experimental data is not much different from earlier assessments and is only discussed very briefly. For only a few cases, for example when new conflicting data exist, will an evaluation of the available experimental data be presented.

The Al–Fe system is important both for commercial alloys and for theoretical studies of ordering transformations. It forms a part of many commercial alloys, which means that the extrapolations to higher-order systems of the stable and metastable ordered forms require accurate modeling of the binary system itself. As there are no experimental data for phases that are not stable in the binary, one must rely on *ab initio* calculations or "backward" extrapolation from ternary systems.

The generally accepted assessed phase diagram for Al–Fe shown in Fig. 1 is from an assessment by Kattner and Burton [1]. The different phases are listed in Table 1. The AlFe (B2) and $AlFe_3(D0_3)$ phases are ordered forms on the body-centered cubic (bcc) lattice and are separated from the disordered A2 phase by first- or second-order

* Corresponding author. Tel.: +33 684330509.
E-mail address: bo.sundman@ensiacet.fr (B. Sundman).

1359-6454/$36.00 © 2009 Acta Materialia Inc. Published by Elsevier Ltd. All rights reserved.
doi:10.1016/j.actamat.2009.02.046

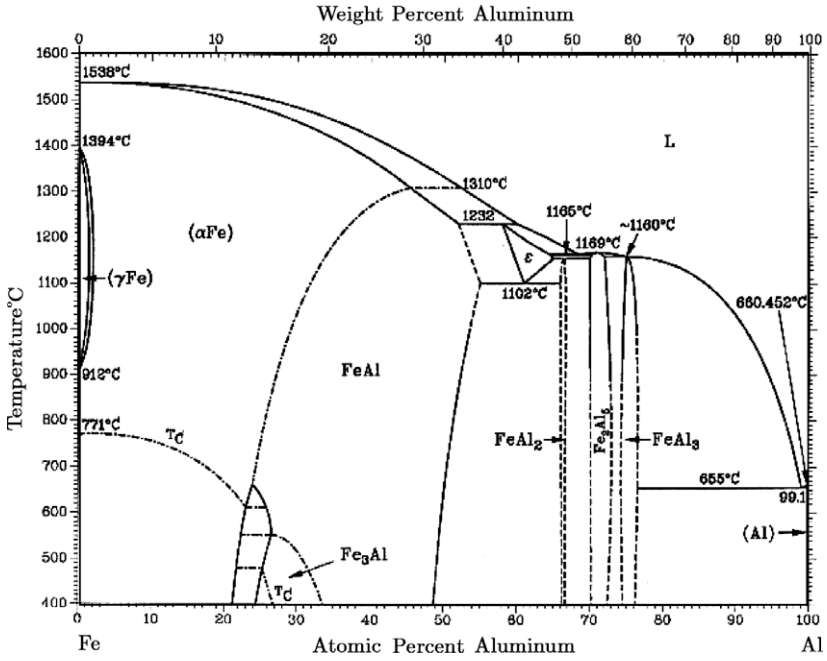

Fig. 1. The Al–Fe phase diagram assessed by Kattner and Burton [1]. See the text for details.

Table 1
Phases and structures.

Phase	Label in Fig. 1	Label in Fig. 2	Struktur Bericht	Pearson symbol	Space group	Prototype
Liquid	L	Liquid	...	...	...	...
fcc	(γFe) or (Al)	A1	A1	cF4	$Fm\bar{3}m$	Cu
bcc	(αFe)	A2(pm) or A2(fm)	A2	cI2	$Im\bar{3}m$	W
AlFe	FeAl	B2(pm)	B2	cP8	$Pm\bar{3}m$	CsCl
$AlFe_3$	Fe_3Al	$D0_3$	$D0_3$	cF16	$Fm\bar{3}m$	BiF_3
Al_8Fe_5	ϵ	Al_8Fe_5	$D8_2$	cI52	$I4\bar{3}m$	Cu_5Zn_8
Al_2Fe	$FeAl_2$	Al_2Fe	...	aP18	P1	$FeAl_2$
Al_5Fe_2	Fe_2Al_5	Al_5Fe_2	...	oC?	Cmcm	...
$Al_{13}Fe_4$	$FeAl_3$	$Al_{13}Fe_4$	...	mC102	C2/m	...

transitions, the latter dash-dotted. There is also a dash-dotted line for the Curie temperature denoted T_C. Some of the solubility lines are dashed because they are not well determined.

Kattner and Burton [1] did not present a set of parameters to calculate the whole diagram as the modeling technique at the time did not allow an acceptable thermodynamic model for the B2 and $D0_3$ ordering. The thermodynamic assessment most used in databases is by Seiersten [2] from the COST 507 project [3]. However, her assessment has never been published together with a comparison with experimental data, and the two-sublattice model used can describe only the B2 ordering, not the $D0_3$ one. There have been several amendments of the assessment by Seiersten to improve various features, but without proper documentation or publication.

In a recent revision of the Seiersten description, Jacobs and Schmid-Fetzer [4] introduced the formation of vacancies in addition to the anti-site defects into the two-sublattice model and found that the use of vacancy defects had no significant effect on the calculated A2/B2 transition. Jacobs and Schmid-Fetzer could not find a description that accurately reproduced the vacancy concentrations observed by Kerl et al. [5] and they used a two-sublattice model for the ordering in the bcc lattice.

The current paper presents a complete revision of the modeling using a four-sublattice model based on the compound energy formalism (CEF) and taking all experimental and theoretical data into account. The calculated phase diagram is shown in Fig. 2. The invariant temperatures are listed in Table 2.

The transitions between the disordered and the different ordered structures can be of first and second order, and this can only be achieved using a single Gibbs energy function. The B2 ordering has the ideal stoichiometry AlFe and the $D0_3$ ordering has the ideal stoichiometry $AlFe_3$ but, as can be seen in the phase diagrams, there are considerable ranges of solubility in both phases. This has been modeled using anti-site defects and, for compatibility with higher-order systems like Al–Fe–Ni, vacancy defects have also

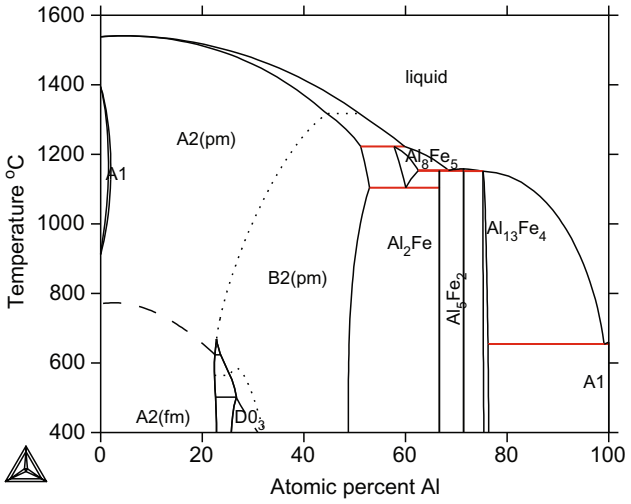

Fig. 2. The calculated Al–Fe phase diagram from the current assessment. The phase regions are labeled according to Table 1. The lines representing second-order transitions between chemically ordered states are short dashed and those between ferro- and paramagnetic states are long dashed.

Table 2
Invariants.

Transformation	T °C [1]	T °C [3]	T °C [6]	T °C [7]	T °C (this work)
liq + B2 → Al_8Fe_5	1232	1222	1231	1222	1226
liq → Al_8Fe_5 + Al_5Fe_2	1169	1157	1155	1155	1154
Al_8Fe_5 + Al_5Fe_2 → Al_2Fe	1165	1155	1146	1155	1153
liq + Al_5Fe_2 → $Al_{13}Fe_4$	1160	1151	1149	1153	1151
Al_8Fe_5 → B2 + Al_2Fe	1102	1115	1092	1094	1089
liq → A1 + $Al_{13}Fe_4$	655	654	–	654	654

been introduced. The modeling of the different ordered forms of the bcc lattice is discussed in Section 3.1 and the fit to various experimental data is discussed in Section 4.

2. Experimental data

The assessment by Kattner and Burton gives a complete review of all experimental data up to 1992. In most cases the same selection of data to be fitted has been followed except for the liquidus in equilibrium with the Al-rich compounds, where the more recent assessment by Du et al. [7] has been used. The new data on the phase diagram have generally confirmed previous data; however, significantly lower enthalpies of formation were found for the thermodynamic data, as shown in Fig. 3 and discussed below.

2.1. New phase diagram data

The experimental data by Ikeda et al. [8] established the shape of the region around $AlFe_3$. Stein and Palm [6] measured the liquidus and solidus and the second-order transitions in bcc, mainly confirming existing data. Although they measured only a few liquidus temperatures in the region with Al fractions between 0.65 and 0.8, their temperatures are in agreement with the assessment by Du et al. [7].

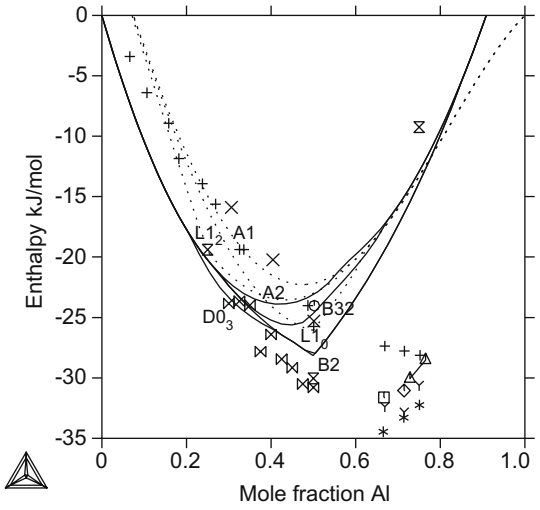

Fig. 3. The full lines are calculated enthalpy of formation at 300 K of several ordered forms of bcc (A2) and the symbols for the calculated Al-rich compounds are □ for Al_2Fe,◇ for Al_5Fe_2 and △ for $Al_{13}Fe_4$. The reference state is bcc for Fe and fcc for Al. The enthalpy curves for face-centered cubic (fcc) (A1) and the ordered $L1_2$ and $L1_0$ are shown as dashed lines. Experimental data are from + [11], × [12], ○ [18], ∗ [19], ϒ [20], ⋈ [10] and *ab initio* data ⧖ from [13] for $D0_3$ and B2 structures.

The crystal structure of the high temperature ϵ phase was determined by Vogel et al. [9] to have the gamma-brass structure $D8_2$ with prototype Cu_5Zn_8.

2.2. New thermochemical data

The calorimetric measurements of Breuer et al. [10] give significantly lower enthalpies of formation of the AlFe B2 phase than the earlier experiments by Oelsen and Middel [11] and Kubaschewski and Dench [12]. The calculated enthalpies of the previous thermodynamic descriptions of the bcc-based phases were lower than the data from these experiments and, in a way, the new experimental data from Breuer et al. confirm what had been found by modeling.

The calculated enthalpies of formation of bcc and the compounds stable at 300 K are shown in Fig. 3. The more recent experiments and the *ab initio* data from Lecherman et al. [13] are included. There are also calculated curves for the metastable A2 and B32 structures, and dashed curves for the A1 and its ordered forms $L1_2$ and $L1_0$.

Kattner and Burton [1] noted that the data for the chemical potential of Al in the A2 phase can be divided into two groups with different slopes. Newer data from Jacobson and Mehrotra [14] agree with the group of data having the flatter slope, while the data from Kleykamp and Glasbrenner [15] and Bencze et al. [16] agree with the data with the steeper slope. Huang et al. [17] determined the chemical potential of Al in the $D0_3$ phase.

2.3. New theoretical data

All *ab initio* calculations have so far found that the stable $D0_3$ ordered form on bcc lattice is less stable than the

$L1_2$ ordered form on fcc lattice and, therefore, the *ab initio* results cannot be used uncritically. The calculated curves for A1 (disordered) and its ordered forms are included as dashed lines in Fig. 3. It should be noted that this assessment gives a minimum difference in the Gibbs energy between $D0_3$ and $L1_2$ of 150 J/mol at 700 K.

The *ab initio* enthalpy value for the metastable $D0_3-Al_3Fe$ is less negative than that for the B2 phase implying that the $D0_3$ ordered Al_3Fe should not be stable even when only the bcc-based phases are considered.

3. Modeling

All the modeling has been based on the CEF as described by Lukas et al. [21]. The molar Gibbs energy is divided into four terms:

$$G_m = {}^{\mathrm{srf}}G_m + {}^{\mathrm{cfg}}G_m + {}^{\mathrm{mgn}}G_m + {}^{E}G_m \tag{1}$$

The first two terms are the "surface of reference" and "configurational" contributions, and for a substitutional regular solution model these are:

$$\begin{aligned} {}^{\mathrm{srf}}G_m &= \sum_i x_i {}^{\circ}G_i(T) \\ {}^{\mathrm{cfg}}G_m &= RT\sum_i x_i \ln(x_i) \end{aligned} \tag{2}$$

where x_i is the mole fraction of component i and ${}^{\circ}G_i$ is the Gibbs energy of the component i as a function of temperature. The configurational term represents the ideal entropy of mixing, the factor R is the gas constant and T is the absolute temperature. The third term in Eq. (1) is the magnetic contribution described in Section 3.2. The fourth term is the excess part and is described by a Redlich–Kister series:

$${}^{E}G_m = x_{\mathrm{Al}}x_{\mathrm{Fe}}\sum_{v=0}(x_{\mathrm{Al}}-x_{\mathrm{Fe}})^v {}^vL_{\mathrm{Al,Fe}} \tag{3}$$

The ${}^vL_{\mathrm{Al,Fe}}$ can be temperature dependent. The bcc and fcc phases have been modelled with four sublattices for ordering. The model for bcc ordering is described in Section 3.1. No stable ordered fcc phases exist in the binary Al–Fe, but these are formed with the addition of Ni, Ti or C. The model for the fcc ordering in Al–Fe is similar to that described here for bcc ordering. Details can be found in the paper on the Al–C–Fe system by Connetable et al. [22].

The three intermediate phases stable at low temperatures on the Al-rich side have been modelled the same way as by Seiersten [2]. The Al_5Fe_2 and Al_2Fe phases are treated as stoichiometric with no solubility ranges, their Gibbs energies depend only on temperature. The $Al_{13}Fe_4$ phase is described with three sublattices: one sublattice is only occupied by Al, the second one is only occupied by Fe and mixing of Al and vacancies occurs on the third.

3.1. Modeling ordering in bcc

The B2 ordering on the bcc lattice can easily be modelled with the two-sublattice CEF model, each sublattice corresponding to a site of crystallographic structure, as shown in Fig. 4(a). These two sites are crystallographically equivalent. Exchanging the occupation of the two sublattices should thus induce an identical energy *i.e.* ${}^{\circ}G_{\mathrm{A:B}} = {}^{\circ}G_{\mathrm{B:A}}$ and ${}^vL_{\mathrm{A,B:i}} = {}^vL_{\mathrm{i:A,B}}$.

When modeling the $D0_3$ ordering, shown in Fig. 4(b), a four-sublattice CEF model is needed. The different sublattices correspond to the edges of the tetrahedra constituting the bcc lattice. These tetrahedra are irregular as they involve first and second nearest neighbors. The four sublattices are thus not equivalent. As a consequence, the ideal order at equiatomic composition can correspond to the B2 ordering where the bonds between different elements are only between first nearest neighbors or to the B32-type ordering, shown in Fig. 4(c), where such bonds are between both first and second nearest neighbors.

In the B2 phase of the Al–Fe system the dominating defects are anti-site atoms, i.e. Al and Fe atoms can occupy all sublattices. Close to the equiatomic composition a small number of the lattice sites are occupied by vacancies. In the binary Al–Ni system, this type of defect is responsible for the extension of the B2 phase up to $x_{\mathrm{Al}} = 0.58$. In order to extend the description to the Al–Fe–Ni system, it is thus important to include vacancies in the model, but this has to be done in the simplest possible way as there are almost no data available for this binary system. Therefore, no ordering between the vacancies and the atoms is considered.

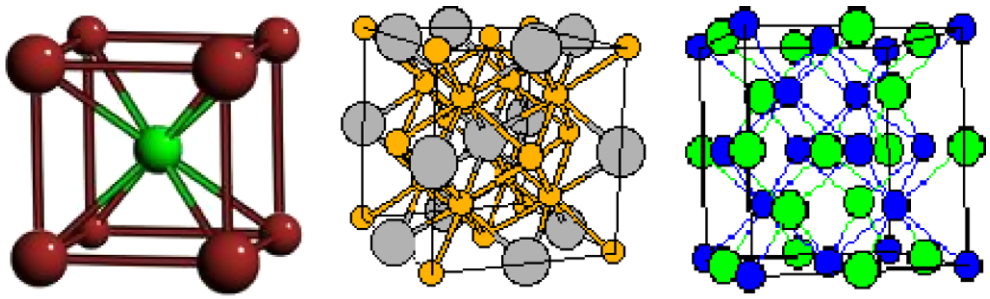

(a) B2 (b) $D0_3$ (c) B32

Fig. 4. The B2, $D0_3$ and B32 structures [23].

The molar Gibbs energy for a phase with four sublattices is divided into the same four parts as Eq. (1) and the first two parts can be written as:

$$^{\mathrm{srf}}G_m = \sum_i \sum_j \sum_k \sum_l y_i^{(1)} y_j^{(2)} y_k^{(3)} y_l^{(4)} {}^{\circ}G_{ijkl}$$
$$^{\mathrm{cfg}}G_m = RT \sum_s a_s \sum_i y_i^{(s)} \ln(y_i^{(s)}) \quad (4)$$

The site fraction $y_i^{(s)}$ gives the fractions of the constituent i in sublattice s and a_s is the number of sites on sublattice s. When the phase is disordered the site fractions of all constituents are equal in all sublattices. The parameter $^{\circ}G_{ijkl}$ is the energy of the configuration $ijkl$ in the four sublattices representing the bcc tetrahedron. There are four bonds between nearest neighbors and two between next nearest neighbors in this tetrahedron. Many configurations thus have the same energy, for example:

$$^{\circ}G_{\mathrm{AlAlAlFe}} = {}^{\circ}G_{\mathrm{AlAlFeAl}} = {}^{\circ}G_{\mathrm{AlFeAlAl}} = {}^{\circ}G_{\mathrm{FeAlAlAl}}.$$

Assuming that the next nearest neighbor bonds are between atoms on sublattices 1 and 2 and between atoms on sublattices 3 and 4, one has

$$^{\circ}G_{\mathrm{AlAlFeFe}} = {}^{\circ}G_{\mathrm{FeFeAlAl}} \quad \text{and}$$
$$^{\circ}G_{\mathrm{AlFeAlFe}} = {}^{\circ}G_{\mathrm{AlFeFeAl}} = {}^{\circ}G_{\mathrm{FeAlAlFe}} = {}^{\circ}G_{\mathrm{FeAlFeAl}}.$$

These parameters are related to the ordered structures: $^{\circ}G_{\mathrm{AlFeFeFe}}$ corresponds to $D0_3$, $^{\circ}G_{\mathrm{FeFeAlAl}}$ to B2 and $^{\circ}G_{\mathrm{FeAlFeAl}}$ to B32.

The excess Gibbs energy term for the sublattice phase can be expanded in Redlich–Kister parameters as for the substitutional model in Eq. (3). In the present work, these terms were taken independent of the occupation in the other sublattices except that where the interaction is considered.

$$\begin{aligned} {}^{E}G_m = {} & y_{\mathrm{Al}}^{(1)} y_{\mathrm{Fe}}^{(1)} \sum_{v=0} (y_{\mathrm{Al}}^{(1)} - y_{\mathrm{Fe}}^{(1)})^v {}^{v}L_{\mathrm{Al,Fe:*:*:*}} \\ & + y_{\mathrm{Al}}^{(2)} y_{\mathrm{Fe}}^{(2)} \sum_{v=0} (y_{\mathrm{Al}}^{(2)} - y_{\mathrm{Fe}}^{(2)})^v {}^{v}L_{\mathrm{*:Al,Fe:*:*}} \\ & + y_{\mathrm{Al}}^{(3)} y_{\mathrm{Fe}}^{(3)} \sum_{v=0} (y_{\mathrm{Al}}^{(3)} - y_{\mathrm{Fe}}^{(3)})^v {}^{v}L_{\mathrm{*:*:Al,Fe:*}} \\ & + y_{\mathrm{Al}}^{(4)} y_{\mathrm{Fe}}^{(4)} \sum_{v=0} (y_{\mathrm{Al}}^{(4)} - y_{\mathrm{Fe}}^{(4)})^v {}^{v}L_{\mathrm{*:*:*:Al,Fe}} \end{aligned} \quad (5)$$

The character "*" in a sublattice means that the parameter is independent of the occupation of that sublattice. The interactions are identical in all sublattices:

$$^{v}L_{\mathrm{Al,Fe:*:*:*}} = {}^{v}L_{\mathrm{*:\ Al,Fe:*:*}} = {}^{v}L_{\mathrm{*:*:\ Al,Fe:*}} = {}^{v}L_{\mathrm{*:*:*:Al,Fe}}.$$

The Gibbs energy for the ordered and disordered forms of bcc are calculated from the same set of parameters. The contribution from the ordering part is added to the description of the disordered state using the following relations.

$$G_m^{\mathrm{total}} = G_m^{\mathrm{dis}}(x) + \Delta G_m^{\mathrm{ord}} \quad (6)$$
$$\Delta G_m^{\mathrm{ord}} = G_m^{\mathrm{subl}}(y) - G_m^{\mathrm{subl}}(y = x) \quad (7)$$

In Eq. (7) $\Delta G_m^{\mathrm{ord}}$ will always be zero when the phase is disordered, i.e. when all site fractions are the same on all sublattices, because the four sublattice Gibbs energy, G^{subl}, is calculated twice with the same set of model parameters: once with the original set of site fractions, y, and a second time with all site fractions equal to the overall composition, x. However, this also means that if care is not taken in assessing the parameters, ordering may occur for the wrong reason, i.e. that $-G_m^{\mathrm{subl}}(y = x)$ is more negative than $G_m^{\mathrm{subl}}(y)$. The Thermo-Calc[1] software, for example, will give a warning when this happens.

Recent modifications to the Thermo-Calc software [24] include automatic handling of the permutations of the same parameter for four-sublattice modeling of fcc, hcp and bcc ordering, thus further reducing the possibility of incorrect use of the model.

3.2. Magnetic model

The magnetic model was proposed by Inden [25] and it contributes to the Gibbs energy according to

$$^{\mathrm{mgn}}G_m = RT\, f(\tau) \ln(\beta + 1) \quad (8)$$

where R is the gas constant, T is the absolute temperature and $f(\tau)$ is the integral of a function fitted to the contribution to the heat capacity due to the magnetic transition. τ is T/T_C where T_C is the Curie temperature and β is the average Bohr magneton number per atom. The composition and ordering dependence of the Curie temperature and the Bohr magneton number is described in the same way as for the Gibbs energy, i.e.

$$T_C^{\mathrm{total}} = T_C^{\mathrm{dis}}(x) + \Delta T_C^{\mathrm{ord}} \quad (9)$$
$$\Delta T_C^{\mathrm{ord}} = T_C^{\mathrm{subl}}(y) - T_C^{\mathrm{subl}}(y = x) \quad (10)$$

The use of Redlich–Kister series are not well suited to describe the Curie temperature and Bohr magneton number as these may very rapidly with composition and can be zero for an extended composition range. However, in order to calculate chemical potentials it is necessary to have a smooth function and thus they are used.

4. Assessment procedure and results

The first Al–Fe phase diagram including $D0_3$ ordering was assessed by Ohnuma [26] but was never published because it had some unsatisfactory features. However, Ohnuma obtained a better A2/B2 transition line than Seiersten [2] and fitted the composition dependence of the Curie temperature better. In order to avoid the miscibility gap between $D0_3$ and B2 on the Al-rich side of $D0_3$, as found by Ohnuma, the present assessment enforced a continuous increase of the chemical potential of Al for x_{Al}

[1] Commercial products are referenced in this paper as examples. Such identification does not imply recommendation or endorsement by the National Institute of Standards and Technology.

between 0.25 and 0.5 at several temperatures. During the assessment, which was attempted on and off during several years, unrealistic shapes of the ordering transformations and changes from second- to first-order A2/B2 transitions had to be corrected by adding constraints on the experimental data and the optimizing parameters in order to force the optimization to reproduce the available data and give reasonable extrapolations.

The current assessment is a balanced result between correctly describing the experimental data and using a reasonable number of adjustable parameters in the models. For example, the steep decrease in the Curie temperature in the $D0_3$ region would require many coefficients to keep the Curie temperature small for $x_{Al} > 0.4$. Instead, a less steep slope was accepted and a single coefficient was used; see also Section 5.

All parameters for all phases have been reassessed in the present work and are listed in the Appendix A. In the final set, the parameters for disordered bcc were so close to those by Seiersten [3] that her parameters were retained because this reduces the number of changes needed in higher-order systems. Due to the use of Eq. (7) to express the ordering contribution, there are an infinite number of equivalent expressions that can be used for the parameters of $G_m^{\text{subl}}(y)$; those listed were chosen in order to minimize the number of parameters.

4.1. Equilibria with the liquid

In Fig. 5(a) the Fe-rich part of the liquidus and solidus is shown together with experimental data. The agreement is good and the maximum difference between the calculated curve and the most recent experimental data by Stein and Palm [6] is 10 K. The calculated liquidus has a maximum at $x_{Al} = 0.05$ and 1814 K.

In the center of the phase diagram, shown in Fig. 5(b), there are four intermediate phases and two of these have been modelled as stoichiometric compounds, Al_2Fe and Al_5Fe_2. The structure of the phase that is only stable at high temperature, often called ϵ or "Al_5Fe_4", has recently been determined by Vogel et al. [9] as Cu_5Zn_8-type (Strukturbericht $D8_2$) and has been modelled with two sublattices with anti-site defects in both, $(Al, Fe)_8(Fe, Al)_5$.

In agreement with the experiments, the Al_8Fe_5 phase forms peritectically at 1226°C and in the assessment the Al_2Fe phase forms 1 degree below the eutectic between Al_8Fe_5 and Al_5Fe_2. The Al_5Fe_2 has congruent melting point. The invariants are listed in Table 2 and are in close agreement with the recent assessment by Du et al. [7]. The liquidus curve between $Al_{13}Fe_4$ and pure Al is well fitted to the experimental data, as shown in Fig. 5(c).

For the liquid, experimental data on the enthalpy of mixing are shown in Fig. 6(a). The agreement with the calculated line is excellent. In Fig. 6(b) the chemical potentials at 1873 K are compared to experimental data; the agreement is again very good.

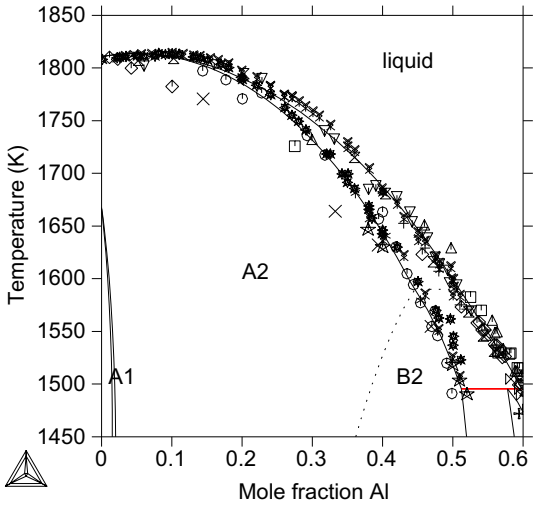

(a)High Fe side

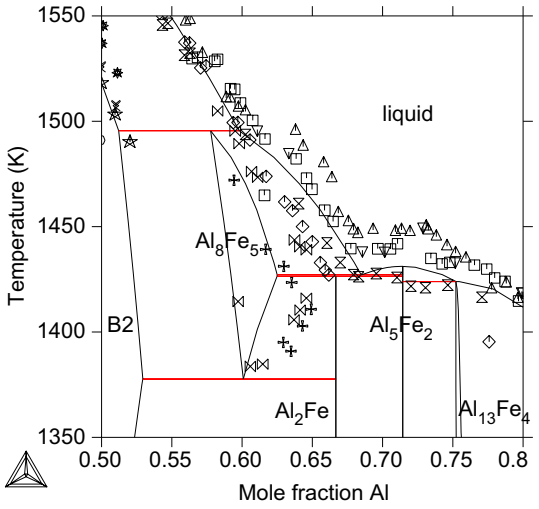

(b)Middle region

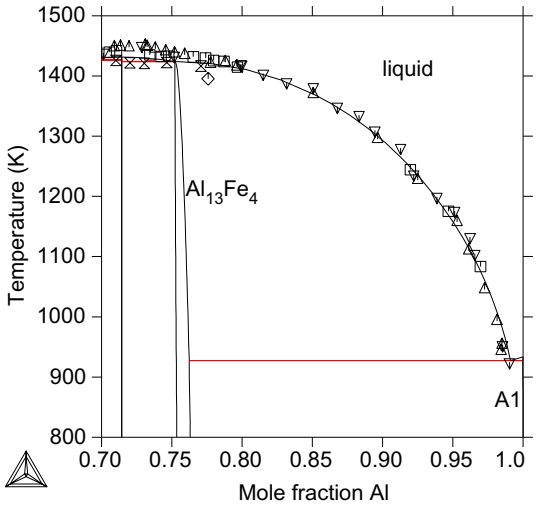

(c)High Al side

Fig. 5. The calculated phase diagram for the liquid in equilibrium with bcc compared with experimental data. In (a) the dashed line is the second-order A2/B2. The invariant temperatures are listed in Table 2. The experimental data for the liquidus are from △ [27], □ [28], ◇ [29], ⧖ [30], ▽ [31], +[32], ϒ [6] and for the solidus are from ⋈ [28], ✠ [29], ∗ [30], × [44], ○ [31], ☆ [32], ⅄ [6].

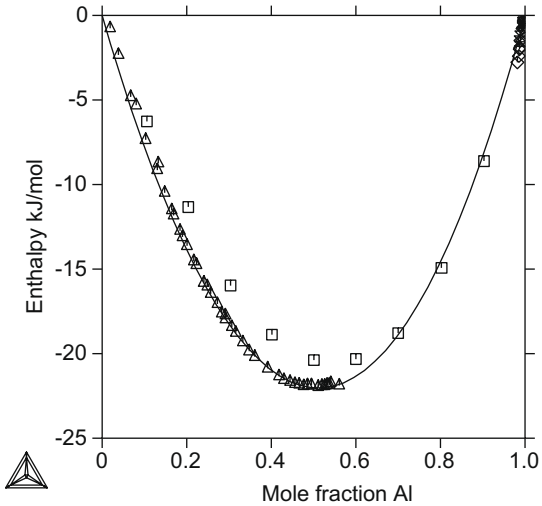

(a) Enthalpy of mixing at 1873 K

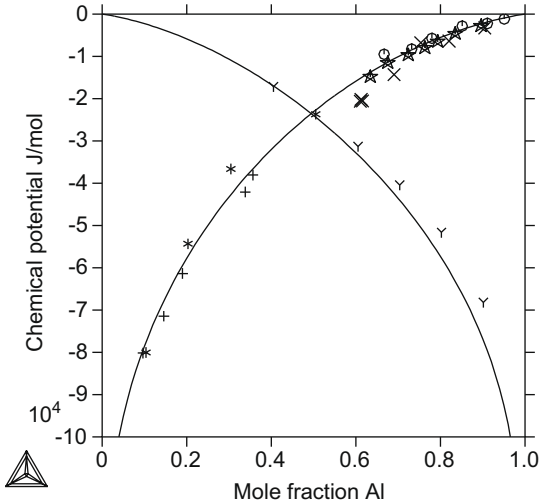

(b) Chemical potentials at 1873 K

Fig. 6. The calculated enthalpy of mixing and chemical potential of the components in the liquid at 1873 K, compared with experimental data from: △ [33], □ [34], ◇ [35], ⧖ [36], ▽ [37]. Chemical potentials for Al are from: + [38], × [39], ○ [40], ∗ [41], ☆ [42], and for Fe are from ϒ [41].

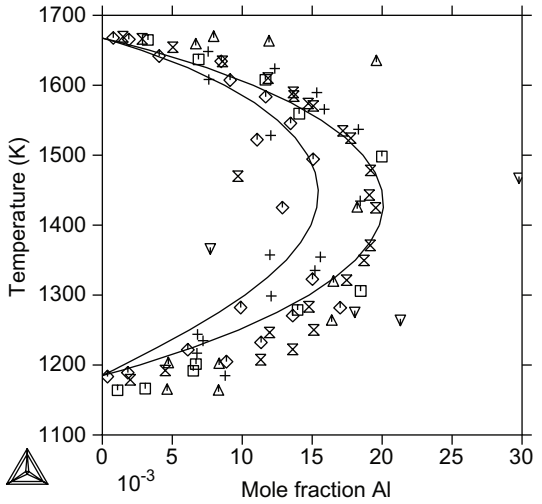

(a) γ loop

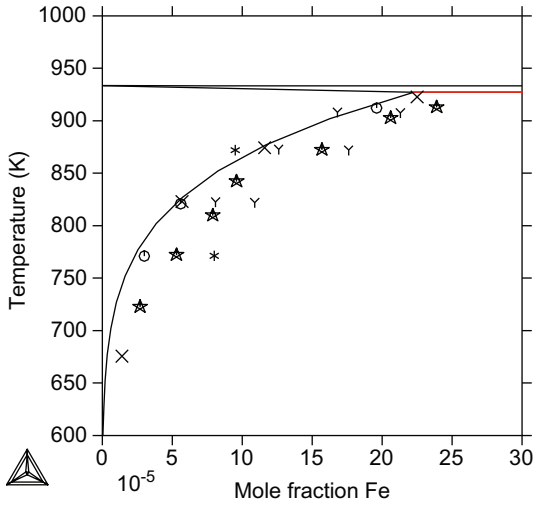

(b) Solubility of Fe in Al

Fig. 7. The calculated γ loop and solubility of Fe in Al compared with experimental data from: △ [29], □ [43], ◇ [44], ⧖ [45], ▽ [46], + [47], ∗ [48], × [49], ○ [50], ★ [51], ⅄ [52].

4.2. Equilibria with the fcc phase

The fcc phase is only stable close to the pure elements: on the Fe side as a so-called γ loop and on the Al side with a very small solubility of Fe. These are shown in Fig. 7, together with experimental data. The metastable ordering in the fcc phase is discussed together with the bcc phase in Section 6.

4.3. Equilibria with ordered and disordered bcc phases

The bcc phase has ordering transformations to B2 and $D0_3$, both of which can be first- or second-order, and a ferromagnetic transition that depends on the composition, all of which are shown in Fig. 8(a)–(c). The full lines are solubility lines, the second-order chemical transitions are short dashed and the ferromagnetic transitions are long dashed. The second-order A2/B2 transition extends up to the melting temperature and the fit of the calculated curve to the experimental data is very good, as shown in Fig. 8(a).

The ferromagnetic transition is shown in Fig. 8(b), together with experimental data. The ferromagnetic transition temperature is considerably decreased when chemical ordering occurs. The fit to the data for the disordered region is excellent, but the calculated Curie temperature for the $D0_3$ phase does not decrease as steeply as indicated by the experimental data. All attempts to improve the fit to the Curie temperature in the $D0_3$ region failed because a steeper slope makes it impossible to fit the phase diagram around the A2/B2/$D0_3$ first- and second-order transitions. A better magnetic model may be needed to improve this, as discussed in Section 5, but the present assessment is limited to what is available in the software.

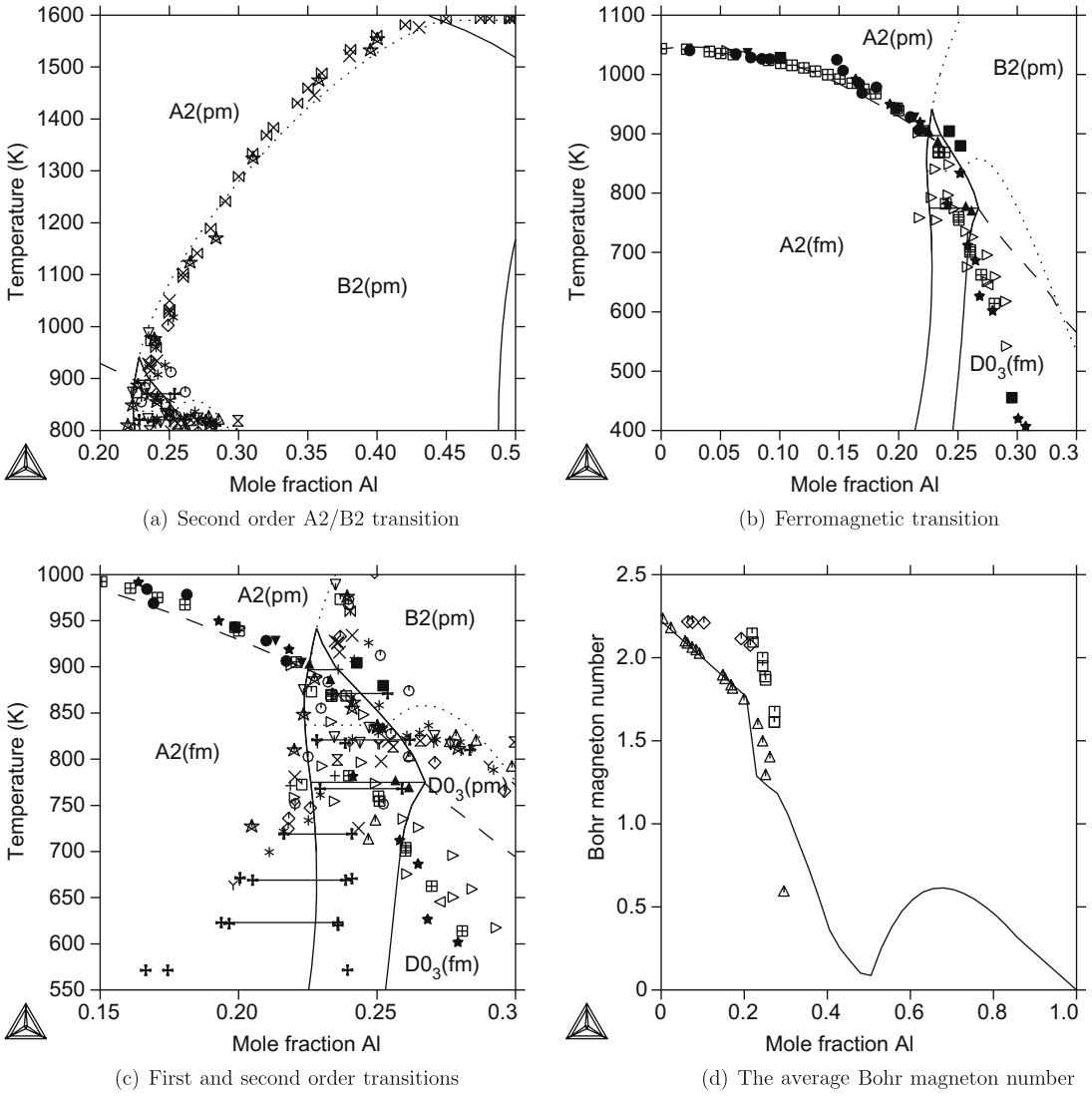

(a) Second order A2/B2 transition

(b) Ferromagnetic transition

(c) First and second order transitions

(d) The average Bohr magneton number

Fig. 8. The calculated first- and second-order transition lines for A2/B2, A2/D0$_3$, B2/D0$_3$ and ferromagnetism together with experimental data. The magnetic transition lines are long dashed, the chemical second-order transition lines are short dashed. Experiments of the A2/B2 ordering are from: △ [53], □ [54], ◇ [55], ⧖ [56], ▽ [57], + [58], ∗ [59], ⋈ [6]. The B2/D0$_3$ ordering experiments are from: ✠ [8], ⋎ [6], × [60], ○ [61], ☆ [62]. The ferromagnetic transitions experiments are from: • [63], ▲ [64], ■ [65], ▼ [66], ▷ [59], ◁ [61], ★ [62], ⊞ [6]. In (d) the calculated Bohr magneton number for A2, B2 and D0$_3$ is shown over the whole composition range. Experimental data are from △ [63], □ [64] and ◇ [65].

In Fig. 8(d) the average Bohr magneton number per atom is shown for the whole composition range and the drastic effect of chemical ordering is evident. Two coefficients were used to describe the composition dependence of the Curie temperature in the disordered bcc and for the ordered state. In the disordered state the Bohr magneton number varies linearly with composition, while in the ordered state four coefficients were used to describe the sharp decrease.

Fig. 8(c) is a magnification of the region where complex first- and second-order transitions occur between the different ordered states A2, B2 and D0$_3$, as well as the ferro- and paramagnetic states. The fit to the experimental data is good and even by using models with a better description of the short-range order contribution to the Gibbs energy, like CVM or Monte Carlo [67,68], the fit has not been any better. The basic features are well reproduced, i.e. the second-order transitions for A2/B2 turns into first-order transitions just before meeting the ferromagnetic transition line. The calculated D0$_3$/B2 second-order transition follows the experimental data, but has a maximum at a slightly higher temperature than the experimental value. The shape of the solubility lines when the second-order transitions opens up to first-order transitions is also close to the experimental data, and the two-phase region between A2 and D0$_3$ extends down to 0 K. However, the solubility of Al in A2 at temperatures below 700 K is higher than the experimental data.

The chemical potential of Al in the bcc phases has been measured at 1273 K for low Al content and is shown in

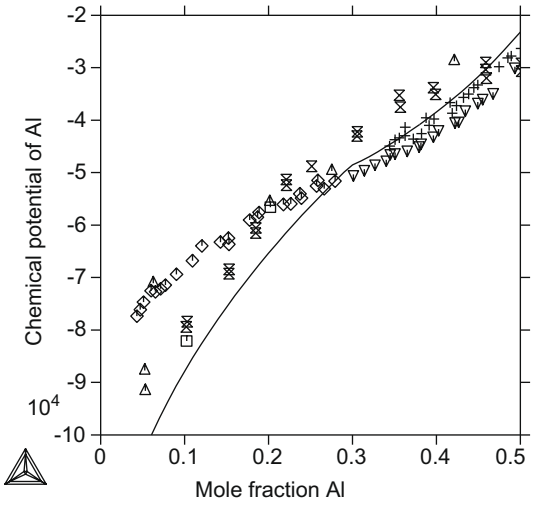

Fig. 9. The calculated chemical potential of Al, referred to fcc, at 1273 K, together with experimental data in A2 from △ [69], □ [19], ◇ [20] and in B2 from ⧖ [19], ▽ [20], and with salt from + [20].

Fig. 9. There are two distinct sets, one showing a rather flat shape [20], while the values in the other set are continuously increasing [69,19]. The calculated curve is closest to the latter. 1273 K is above the ordering temperature for $D0_3$ and there is no reason to have a flat curve for the chemical potential around $x_{Al} = 0.25$; rather, the contrary would be the case if there were any remaining short-range order in the bcc phase.

The variation in the site fractions representing different ordered states in bcc as a function of the composition for a fixed temperature and with the temperature for a fixed composition is shown in Fig. 10. In Fig. 10(a) the diagonal represents the disordered state with the same fractions in all four sublattices. When the $D0_3$ phase forms, the Al fraction in sublattice 1 increases rapidly and then decreases, while in sublattice 2 the Al fraction first decreases but then increases. The two remaining sublattices have the same low fraction of Al until 50% Al. Around 40% Al the $D0_3$ transforms to B2 when sublattices 1 and 2 are of the same fraction. On the Al-rich side there is no $D0_3$ ordering. In Fig. 10(b) the $D0_3$ ordering is stable at 0 K, but around 800 K it becomes B2 and is finally disordered.

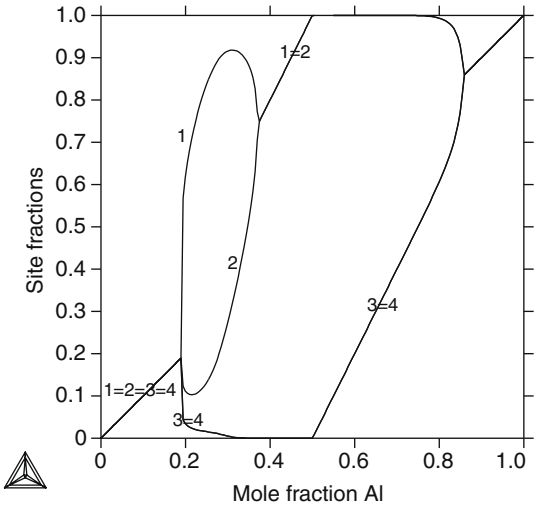

(a) Site fractions at 300 K

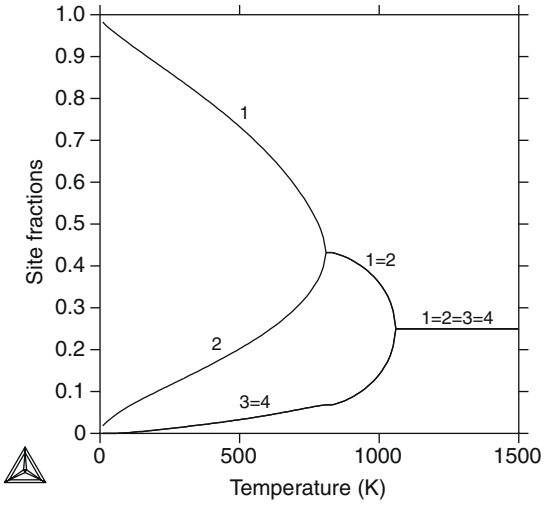

(b) Site fractions at x_{Al} =0.25

Fig. 10. The site fractions in the ordered and disordered bcc phases: (a) for 300 K across the whole system; (b) for $x_{Al} = 0.25$ from 0 to 1500 K. The numbers represent the sublattices.

5. Influence of the ordering on the Curie temperature

According to the experimental information, the Curie temperature changes drastically with the ordering transformation, as shown in Fig. 8(b). It has not been possible to fit such a drastic change; one reason for this may be that the model used for the ferromagnetic transition overestimates the magnetic contribution to the Gibbs energy when the Curie temperature is small. If the Curie temperature is assumed to be independent of ordering, i.e. setting ΔT_C^{ord} in Eq. (9) equal to zero, the phase diagram around $x_{Al} = 0.25$ and $T = 700$ K changes drastically, as shown in Fig. 11. The same region using the assessed value of ΔT_C^{ord} is shown in Fig. 12(a).

6. Phase diagram with only bcc- or fcc-based phases

In Fig. 12 the phase diagram with different ordered forms based on the bcc lattice is shown, all other phases being suppressed. On the Al-rich side there is only B2 ordering, in accordance with *ab initio* results [13].

A persistent problem during this assessment was that, even when the experimental data were well fitted, first-order transitions occurred between the B2 and $D0_3$ ordered phases for mole fractions of Al between 0.35 and 0.45. Even in the present assessment it has been impossible to avoid such phenomena completely, but the remaining nar-

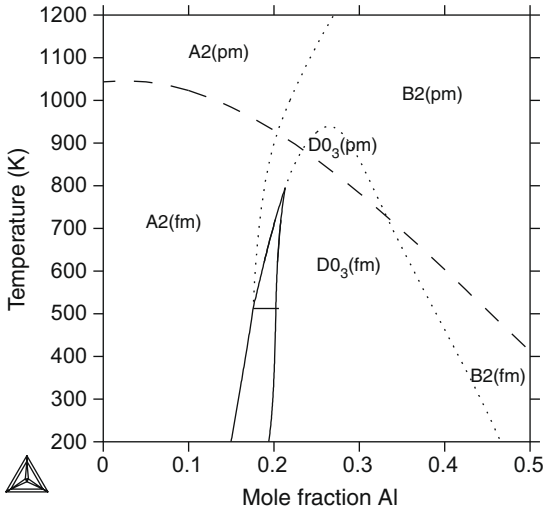

Fig. 11. The calculated phase diagram when ignoring the effect on the Curie temperature by the chemical ordering.

row first-order transition between B2 and $D0_3$ on the high Al side shown in Fig. 12 is probably impossible to verify or refute by experiments or theory.

There are no experimental data for the fcc phase except at the limits of the phase diagram; however, for extrapolations to higher-order systems it is important to have knowledge of the properties of the fcc phase also at higher Al content. Additionally, as there is ordering transformations in the bcc phase it is likely that there are ordering tendencies also in the metastable fcc phase. This is confirmed by *ab initio* calculations.

A reassessment of the fcc phase in Al–Fe, including the ordering, became necessary during a recent assessment of the Al–C–Fe system [22]. This description will also be used in the present work. The metastable phase diagram for the fcc phase is shown in Fig. 12(b). No $L1_2$ ordering but a miscibility gap occurs on the Al-rich side. A four-sublattice CEF model was used and the energy of formation of the $L1_2$ and $L1_0$ phases were fitted to *ab initio* data by Lecherman et al. [13] and Connetable et al. [70].

7. Using a two-sublattice model for bcc-based phases

The present model can be reduced to two sublattices, but then the $D0_3$ ordering is not described. The phase diagram for this case is shown in Fig. 13. This model is sufficient for calculations for temperatures above 900 K and could be easier to apply in more complex calculations, e.g. diffusion simulations.

It is interesting to note that the Gibbs energies of formation of the two $D0_3$ compounds (Al_3Fe and $AlFe_3$) enter as regular parameters in the two-sublattice model, and their difference to the bond energies assessed for B2 and B32 appear in the reciprocal parameter (see the bcc-2SL phase in the Appendix A).

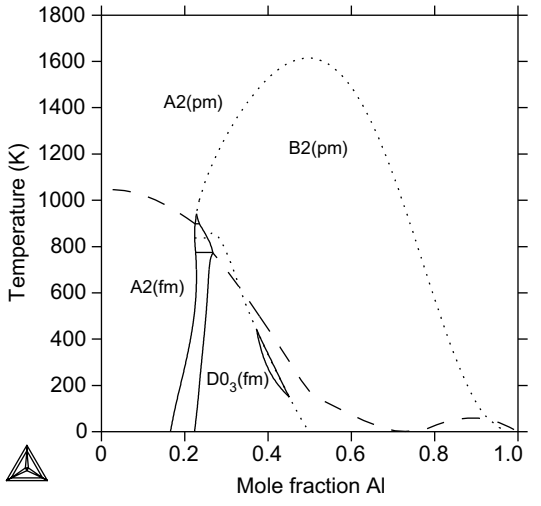

(a) Phase diagram with only bcc based phases

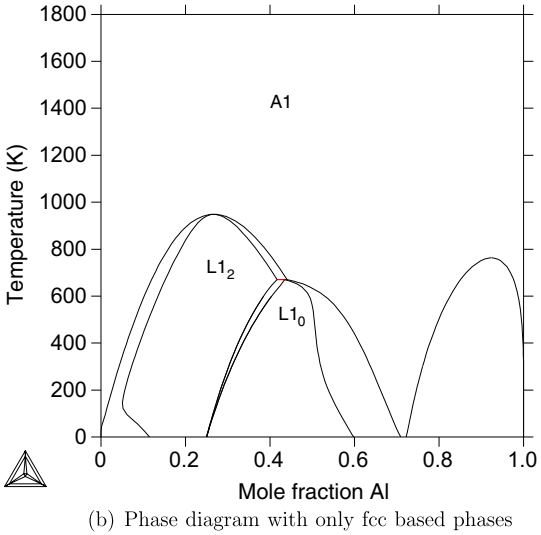

(b) Phase diagram with only fcc based phases

Fig. 12. The calculated phase diagrams for bcc and fcc with all other phases suspended. (a) All phases except the disordered and ordered variants of bcc lattice down to 0 K. The second-order transitions are short dashed and the ferromagnetic transitions are long dashed. Note that the small first-order transition along the B2/$D0_3$ second-order transition exists between 200 and 400 K only. (b) The different fcc-based ordered forms. The $L1_2$ phase should be almost stable as *ab initio* calculations always finds it more stable than the $D0_3$ phase.

8. Conclusion

A four-sublattice CEF-based model has been used to describe the stable and metastable equilibria in the Al–Fe system. The overall fit to experimental and theoretical data is very good. The extrapolations of the fcc and bcc phases in the metastable ranges are reasonable. This confirms that CEF can describe very complex transitions between first- and second-order transformations. The new set of parameters has been tested in several ternary systems, such as Al–C–Fe, Al–Fe–Ni and Al–Fe–Ti, and gives reasonable extrapolations using existing assessments of the other binary systems and small ternary parameters.

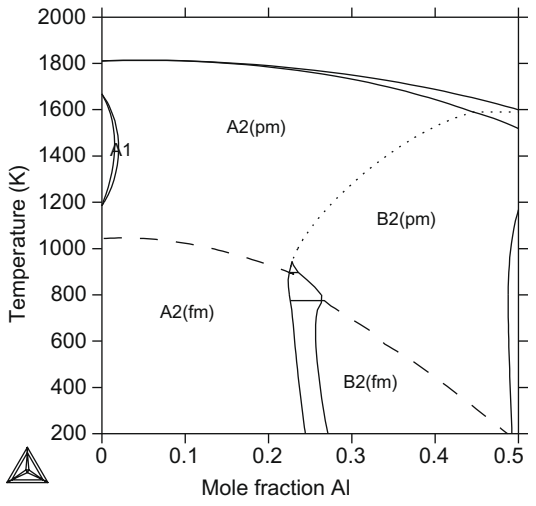

Fig. 13. The phase diagram up to 50 at% Al with the two-sublattice model for bcc. The rest is the same as previously. Note that the A2/B2 first-order transition now bends towards Al, which is as expected because removing the $D0_3$ phase should extend the A2 region.

Acknowledgement

The authors are grateful for inspiration and many useful discussions within the COST 535 action THALU.

Appendix A

List of parameters for the Al–Fe assessment. See Section 3 for the relevant equations. Note that a star "$*$" as a constituent in a sublattice means that the parameter is independent of the constituents in this sublattice. The unary parameters are from SGTE [71].

liquid (Al,Fe)

$$^{\circ}G^{\text{liquid}}_{\text{Al}} - {}^{\circ}H^{\text{fcc-A1}}_{\text{Al}} = +\text{GALLIQ}$$
$$^{\circ}G^{\text{liquid}}_{\text{Fe}} - {}^{\circ}H^{\text{bcc-A2}}_{\text{Fe}} = +\text{GFELIQ}$$
$$^{0}L^{\text{liquid}}_{\text{Al,Fe}} = -88,090 + 19.8\,T$$
$$^{1}L^{\text{liquid}}_{\text{Al,Fe}} = -3800 + 3\,T$$
$$^{2}L^{\text{liquid}}_{\text{Al,Fe}} = -2000$$

fcc-A1 (Al,Fe)

$$^{\circ}G^{\text{fcc-A1}}_{\text{Al}} - {}^{\circ}H^{\text{fcc-A1}}_{\text{Al}} = +\text{GHSERAL}$$
$$^{\circ}G^{\text{fcc-A1}}_{\text{Fe}} - {}^{\circ}H^{\text{bcc-A2}}_{\text{Fe}} = +\text{GFEFCC}$$
$$^{\circ}T^{\text{fcc-A1}}_{C_{\text{Fe}}} = -201$$
$$^{\circ}\beta^{\text{fcc-A1}}_{\text{Fe}} = -2.1$$
$$^{0}L^{\text{fcc-A1}}_{\text{Al,Fe}} = -104,700 + 30.65\,T$$
$$^{1}L^{\text{fcc-A1}}_{\text{Al,Fe}} = +30,000 - 7\,T$$
$$^{2}L^{\text{fcc-A1}}_{\text{Al,Fe}} = +32,200 - 17\,T$$

bcc-A2 (Al,Fe).

This phase is the disordered contribution for the bcc-based phases. It has to be combined to the bcc-4SL or bcc-B2 contribution as indicated by Eqs. (6), (7) to describe the ordered phases.

$$^{\circ}G^{\text{bcc-A2}}_{\text{Al}} - {}^{\circ}H^{\text{fcc-A1}}_{\text{Al}} = +\text{GALBCC}$$
$$^{\circ}G^{\text{bcc-A2}}_{\text{Fe}} - {}^{\circ}H^{\text{bcc-A2}}_{\text{Fe}} = +\text{GHSERFE}$$
$$^{\circ}T^{\text{bcc-A2}}_{C_{\text{Fe}}} = 1043$$
$$^{\circ}\beta^{\text{bcc-A2}}_{\text{Fe}} = 2.22$$
$$^{0}L^{\text{bcc-A2}}_{\text{Al,Fe}} = -122,960 + 32\,T$$
$$^{1}L^{\text{bcc-A2}}_{\text{Al,Fe}} = 2945.2$$
$$^{0}T^{\text{bcc-A2}}_{C_{\text{Al,Fe}}} = -438$$
$$^{1}T^{\text{bcc-A2}}_{C_{\text{Al,Fe}}} = -1720$$

Adding substitutional vacancies to the bcc-A2 phase requires the following three parameters. The first is an estimated energy to create vacancy defects in the bcc lattice; the other two have been estimated from the Al–Fe–Ni system.

$$^{\circ}G^{\text{bcc-A2}}_{\text{Va}} = +30\,T$$
$$^{0}L^{\text{bcc-A2}}_{\text{Al,Va}} = 46,912$$
$$^{0}L^{\text{bcc-A2}}_{\text{Fe,Va}} = 150,000$$

$$\mathbf{Al_{13}Fe_4}(\text{Al})_{.6275}(\text{Fe})_{.235}(\text{Al, Va})_{.1375}$$

$$^{\circ}G^{\text{Al}_{13}\text{Fe}_4}_{\text{Al:Fe:Al}} - 0.765\,{}^{\circ}H^{\text{fcc-A1}}_{\text{Al}} - 0.235\,{}^{\circ}H^{\text{bcc-A2}}_{\text{Fe}} = -30,680 + 7.4\,T + .765\,\text{GHSERAL} + .235\ \text{GHSERFE}$$
$$^{\circ}G^{\text{Al}_{13}\text{Fe}_4}_{\text{Al:Fe:VA}} - 0.6275\,{}^{\circ}H^{\text{fcc-A1}}_{\text{Al}} - 0.235\,{}^{\circ}H^{\text{bcc-A2}}_{\text{Fe}} = -28,100 + 7.4\,T + .6275\,\text{GHSERAL} + .235\ \text{GHSERFE}$$

$$\mathbf{Al_2Fe}(\text{Al})_2(\text{Fe})_1$$

$$^{\circ}G^{\text{Al}_2\text{Fe}}_{\text{Al:Fe}} - 2\,{}^{\circ}H^{\text{fcc-A1}}_{\text{Al}} - {}^{\circ}H^{\text{bcc-A2}}_{\text{Fe}} = -104,000 + 23\,T + 2\,\text{GHSERAL} + \text{GHSERFE}$$

$$\mathbf{Al_5Fe_2}(\text{Al})_5(\text{Fe})_2$$

$$^{\circ}G^{\text{Al}_5\text{Fe}_2}_{\text{Al:Fe}} - 5\,{}^{\circ}H^{\text{fcc-A1}}_{\text{Al}} - 2\,{}^{\circ}H^{\text{bcc-A2}}_{\text{Fe}} = -235,600 + 54\,T + 5\,\text{GHSERAL} + 2\,\text{GHSERFE}$$

$$\mathbf{Al_8Fe_5} - \mathbf{D}82(\text{Al, Fe})_8(\text{Al, Fe})_5$$

$$^{\circ}G^{\text{Al}_8\text{Fe}_5-\text{D82}}_{\text{Al:Al}} - 13\,{}^{\circ}H^{\text{fcc-A1}}_{\text{Al}} = +13\,\text{GALBCC}$$
$$^{\circ}G^{\text{Al}_8\text{Fe}_5-\text{D82}}_{\text{Fe:Al}} - 5\,{}^{\circ}H^{\text{fcc-A1}}_{\text{Al}} - 8\,{}^{\circ}H^{\text{bcc-A2}}_{\text{Fe}} = +200,000 + 36\,T + 5\,\text{GALBCC} + 8\ \text{GHSERFE}$$
$$^{\circ}G^{\text{Al}_8\text{Fe}_5-\text{D82}}_{\text{Al:Fe}} - 8\,{}^{\circ}H^{\text{fcc-A1}}_{\text{Al}} - 5\,{}^{\circ}H^{\text{bcc-A2}}_{\text{Fe}} = -394,000 + 36\,T + 8\,\text{GALBCC} + 5\,\text{GHSERFE}$$
$$^{\circ}G^{\text{Al}_8\text{Fe}_5-\text{D82}}_{\text{Fe:Fe}} - 13\,{}^{\circ}H^{\text{bcc-A2}}_{\text{Fe}} = +13\,\text{GHSERFE} + 13,000$$
$$^{0}L^{\text{Al}_8\text{Fe}_5-\text{D82}}_{\text{Al:Al,Fe}} = -100,000$$
$$^{0}L^{\text{Al}_8\text{Fe}_5-\text{D82}}_{\text{Al,Fe:Fe}} = -174,000$$

$$\mathbf{bcc-4SL}\ (\text{Al, Fe})_{.25}(\text{Al, Fe})_{.25}(\text{Al, Fe})_{.25}(\text{Al, Fe})_{.25}$$

Note that this phase has a contribution from the disordered part bcc-A2. Parameters that are identical for symmetry reason are listed only once.

$${}^{\circ}G^{\text{bcc-4SL}}_{\text{Al:Al:Al:Al}} = +\text{ZERO}$$
$${}^{\circ}G^{\text{bcc-4SL}}_{\text{Al:Al:Al:Fe}} = +\text{ GD03ALFE}$$
$${}^{\circ}G^{\text{bcc-4SL}}_{\text{Al:Fe:Al:Fe}} = +\text{GB32ALFE}$$
$${}^{\circ}G^{\text{bcc-4SL}}_{\text{Al:Fe:Fe:Fe}} = +\text{GD03FEAL}$$
$${}^{\circ}G^{\text{bcc-4SL}}_{\text{Al:Al:Fe:Fe}} = +\text{ GB2ALFE}$$
$${}^{\circ}G^{\text{bcc-4SL}}_{\text{Fe:Fe:Fe:Fe}} = +\text{ZERO}$$
$${}^{\circ}T^{\text{bcc-4SL}}_{C_{\text{Al:Al:Al:Fe:}}} = 4\ \text{UTCALFE}$$
$${}^{\circ}T^{\text{bcc-4SL}}_{C_{\text{Al:Al:Fe:Fe}}} = 6\ \text{UTCALFE}$$
$${}^{\circ}T^{\text{bcc-4SL}}_{C_{\text{Al:Fe:Al:Fe}}} = 5\ \text{UTCALFE}$$
$${}^{\circ}T^{\text{bcc-4SL}}_{C_{\text{Al:Fe:Fe:Fe}}} = 4\ \text{UTCALFE}$$
$${}^{\circ}\beta^{\text{bcc-4SL}}_{\text{Al:Al:Al:Fe}} = \text{ UBMALFE} - 3\ \text{BM0ALFE}$$
$${}^{\circ}\beta^{\text{bcc-4SL}}_{\text{Al:Al:Fe:Fe}} = 2\ \text{UBMALFE} - 4\ \text{BM0ALFE}$$
$${}^{\circ}\beta^{\text{bcc-4SL}}_{\text{Al:Fe:Al:Fe}} = \text{ UBMALFE} - 4\ \text{BM0ALFE}$$
$${}^{\circ}\beta^{\text{bcc-4SL}}_{\text{Al:Fe:Fe:Fe}} = \text{ UBMALFE} - 3\ \text{BM0ALFE}$$
$${}^{1}L^{\text{bcc-4SL}}_{\text{Al,Fe:*:*:*}} = \text{ L1ALFE}$$
$${}^{2}L^{\text{bcc-4SL}}_{\text{Al,Fe:*:*:*}} = \text{ L2ALFE}$$
$${}^{1}\beta^{\text{bcc-4SL}}_{\text{Al,Fe:*:*:*}} = \text{ BM1ALFE}$$
$${}^{2}\beta^{\text{bcc-4SL}}_{\text{Al,Fe:*:*:*}} = \text{ BM2ALFE}$$

fcc − 4SL $(\text{Al},\text{Fe})_{.25}(\text{Al},\text{Fe})_{.25}(\text{Al},\text{Fe})_{.25}(\text{Al},\text{Fe})_{.25}$

Note that this phase has a contribution from the disordered part fcc-A1. Parameters that are identical for symmetry reason are listed only once.

$${}^{\circ}G^{\text{fcc-4SL}}_{\text{Al:Al:Al:Al}} = +\text{ZERO}$$
$${}^{\circ}G^{\text{fcc-4SL}}_{\text{Fe:Al:Al:Al}} = +\text{GAL3FE}$$
$${}^{\circ}G^{\text{fcc-4SL}}_{\text{Fe:Fe:Al:Al}} = +\text{GAL2FE2}$$
$${}^{\circ}G^{\text{fcc-4SL}}_{\text{Fe:Fe:Fe:Al}} = +\text{GALFE3}$$
$${}^{\circ}G^{\text{fcc-4SL}}_{\text{Fe:Fe:Fe:Fe}} = +\text{ZERO}$$
$${}^{0}L^{\text{fcc-4SL}}_{\text{Al,Fe:Al,Fe:*:*}} = +\text{SFALFE}$$

bcc − 2SL $(\text{Al},\text{Fe})_{.5}(\text{Al},\text{Fe})_{.5}$

This phase can be used instead of bcc-4SL if $D0_3$ ordering can be ignored. Note that this phase has a contribution from the disordered part, bcc-A2, and that all permutations of identical parameters are listed.

$${}^{\circ}G^{\text{bcc-2SL}}_{\text{Al:Al}} = +\text{ZERO}$$
$${}^{\circ}G^{\text{bcc-2SL}}_{\text{Fe:Al}} = +2\ \text{GB2ALFE}$$
$${}^{\circ}G^{\text{bcc-2SL}}_{\text{Al:Fe}} = +2\ \text{GB2ALFE}$$
$${}^{\circ}G^{\text{bcc-2SL}}_{\text{Fe:Fe}} = +\text{ZERO}$$
$${}^{\circ}T^{\text{bcc-2SL}}_{C_{\text{Fe:Al}}} = +4\ \text{UTCALFE}$$
$${}^{\circ}T^{\text{bcc-2SL}}_{C_{\text{Al:Fe}}} = +4\ \text{UTCALFE}$$
$${}^{\circ}\beta^{\text{bcc-2SL}}_{\text{Fe:Al}} = +4\ \text{ UBMALFE} - 2\ \text{BM0ALFE}$$
$${}^{\circ}\beta^{\text{bcc-2SL}}_{\text{Al:Fe}} = +4\ \text{ UBMALFE} - 2\ \text{BM0ALFE}$$
$${}^{0}L^{\text{bcc-2SL}}_{\text{Al,Fe:Al}} = +2\ \text{GD03ALFE}$$
$${}^{0}L^{\text{bcc-2SL}}_{\text{Al:Al,Fe}} = +2\ \text{GD03ALFE}$$
$${}^{0}L^{\text{bcc-2SL}}_{\text{Fe:Al,Fe}} = +2\ \text{GD03FEAL}$$
$${}^{0}L^{\text{bcc-2SL}}_{\text{Al,Fe:Fe}} = +2\ \text{GD03FEAL}$$
$${}^{0}L^{\text{bcc-2SL}}_{\text{Al,Fe:Al,Fe}} = -4\ \text{AD03ALFE} - 4\ \text{AD03FEAL}$$
$${}^{1}L^{\text{bcc-2SL}}_{\text{Al,Fe:*}} = +2\ \text{L1ALFE}$$
$${}^{1}L^{\text{bcc-2SL}}_{\text{*:Al,Fe}} = +2\ \text{L1ALFE}$$
$${}^{2}L^{\text{bcc-2SL}}_{\text{*:Al,Fe}} = +2\ \text{L2ALFE}$$
$${}^{2}L^{\text{bcc-2SL}}_{\text{Al,Fe:*}} = +2\ \text{L2ALFE}$$
$${}^{1}\beta^{\text{bcc-2SL}}_{\text{Al,Fe:*}} = +2\ \text{BM1ALFE}$$
$${}^{1}\beta^{\text{bcc-2SL}}_{\text{*:Al,Fe}} = +2\ \text{BM1ALFE}$$
$${}^{2}\beta^{\text{bcc-2SL}}_{\text{Al,Fe:*}} = +2\ \text{BM2ALFE}$$
$${}^{2}\beta^{\text{bcc-2SL}}_{\text{*:Al,Fe}} = +2\ \text{BM2ALFE}$$

Functions

$$\text{R} = 8.31451$$

$$\text{GALLIQ} = \begin{cases} 298.15 \leqslant T < 933.47 : +11005.029 - 11.841867\,T \\ \qquad +7.934\cdot 10^{-20}\,T^{7} + \text{GHSERAL} \\ 933.47 \leqslant T < 6000.00 : +10482.382 - 11.253974\,T \\ \qquad +1.231\cdot 10^{28}\,T^{-9} + \text{GHSERAL} \end{cases}$$

$$\text{GFELIQ} = \begin{cases} 298.15 \leqslant T < 1811.00 : +12040.17 - 6.55843\,T \\ \qquad -3.6751551\cdot 10^{-21}\,T^{7} + \text{GHSERFE} \\ 1811.00 \leqslant T < 6000.00 : -10839.7 + 291.302\,T - 46\,T\ln(T) \end{cases}$$

$$\text{GHSERAL} = \begin{cases} 298.15 \leqslant T < 700.00 : -7976.15 + 137.093038\,T - 24.3671976\,T\ln(T) \\ \qquad -0.001884662\,T^{2} - 8.77664\cdot 10^{-7}\,T^{3} + 74092\,T^{-1} \\ 700.00 \leqslant T < 933.47 : -11276.24 + 223.048446\,T - 38.5844296\,T\ln(T) \\ \qquad +0.018531982\,T^{2} - 5.764227\cdot 10^{-6}\,T^{3} + 74092\,T^{-1} \\ 933.47 \leqslant T < 2900.00 : -11278.378 + 188.684153\,T \\ \qquad -31.748192\,T\ln(T) - 1.230524\cdot 10^{28}\,T^{-9} \end{cases}$$

$$\text{GFEFCC} = \begin{cases} 298.15 \leqslant T < 1811.00 : -1462.4 + 8.282\,T - 1.15\,T\ln(T) \\ \qquad +6.4\cdot 10^{-4}\,T^{2} + \text{GHSERFE} \\ 1811.00 \leqslant T < 6000.00 : -27097.396 + 300.25256\,T \\ \qquad -46\,T\ln(T) + 2.78854\cdot 10^{31}\,T^{-9} \end{cases}$$

$$\text{GALBCC} = +10083 - 4.813\,T + \text{GHSERAL}$$

$$\text{GHSERFE} = \begin{cases} 298.15 \leqslant T < 1811.00 : +1225.7 + 124.134\,T \\ \qquad -23.5143\,T\ln(T) - .00439752\,T^{2} \\ \qquad -5.8927\cdot 10^{-8}\,T^{3} + 77359\,T^{-1} \\ 1811.00 \leqslant T < 6000.00 : -25383.581 + 299.31255\,T \\ \qquad -46\,T\ln(T) + 2.29603\cdot 10^{31}\,T^{-9} \end{cases}$$

$$\text{UBALFE1} = -4023 - 1.14\,T$$
$$\text{UBALFE2} = -1973 - 2\,T$$
$$\text{AD03ALFE} = +3900$$
$$\text{AD03FEAL} = -70 + 0.5\,T$$
$$\text{GB2ALFE} = +4\,\text{UBALFE1}$$
$$\text{GB32ALFE} = +2\,\text{UBALFE1} + 2\,\text{UBALFE2}$$
$$\text{GD03ALFE} = +2\,\text{UBALFE1} + \text{UBALFE2} + \text{AD03ALFE}$$
$$\text{GD03FEAL} = +2\,\text{UBALFE1} + \text{UBALFE2} + \text{AD03FEAL}$$
$$\text{L1ALFE} = -634 + 0.68\,T$$
$$\text{L2ALFE} = -190$$
$$\text{UTCALFE} = -125$$
$$\text{UBMALFE} = -1.36$$
$$\text{BM0ALFE} = -0.3$$
$$\text{BM1ALFE} = -0.8$$
$$\text{BM2ALFE} = +0.2$$
$$\text{UFALFE} = -4000 + T$$
$$\text{GAL3FE} = +3\,\text{UFALFE} + 9000$$

GAL2FE2 = +4 UFALFE
GALFE3 = +3 UFALFE − 3500
SFALFE = +UFALFE
ZERO = 0.0

Appendix B. Supplementary data

Supplementary thermodynamic database file associated with this article can be found, in the online version, at doi:10.1016/j.actamat.2009.02.046.

References

[1] Kattner UR, Burton BP. In: Okamoto H, editor. Phase diagrams of binary iron alloys. Materials Park, OH: ASM International; 1993. p. 12–28.
[2] Seiersten M. SINTEF report STF-28F93051, Oslo, Norway, 1993.
[3] Seiersten M. In: Ansara I, Dinsdale AT, Rand MH. editors. COST 507, Thermochemical Database for Light Metal Alloys, vol. 2. Luxembourg: Office for Official Publications of the European Communities; 1998.
[4] Jacobs MHG, Schmid-Fetzer R. Calphad 2009;33:170–8.
[5] Kerl R, Wolff J, Hehenkamp Th. Intermetallics 1999;7:301–8.
[6] Stein F, Palm M. Int J Mat Res 2007;98:580–8.
[7] Du Y, Schuster JC, Liu Z-K, Hu R, Nash P, Sun W, et al. Intermetallics 2008;16:554–70.
[8] Ikeda O, Ohnuma I, Kainuma R, Ishida K. Intermetallics 2001;9:755–61.
[9] Vogel SC, Eumann M, Palm M, Stein F. COST 535 (THALU) final meeting, Interlaken Switzerland, 2008.
[10] Breuer J, Grün A, Sommer F, Mittemeijer EJ. Metall Mater Trans B 2001;32B:913–8.
[11] Oelsen W, Middel W. Eisenforschung 1937;19:1–26.
[12] Kubaschewski O, Dench WA. Acta Metall 1955;3:339–46.
[13] Lechermann F, Fähnle M, Sanchez JM. Intermetallics 2005;13:1096–109.
[14] Jacobson NS, Mehrotra GM. Metall Trans B 1993;24B:481–6.
[15] Kleykamp H, Glasbrenner H. Z Metallkd 1997;88:230–5.
[16] Bencze L, Raj DD, Kath D, Oates WA, Herrmann J, Singheiser L, et al. Metall Mater Trans A 2003;34A:2409–19.
[17] Huang Y, Yuan W, Qiao Z, Semenova O, Bester G, Ipser H. J Alloy Compd 2008;458:277–81.
[18] Ferro R. Atti Acad Naz Lincei Rend Classe Sci Fis Mat Nat 1963;36:653–8.
[19] Radcliffe SV, Averbach BL, Cohen M. Acta Metall 1961;9:169–76.
[20] Eldridge J, Komarek KL. Trans AIME 1964;230:226–33.
[21] Lukas HL, Fries SG, Sundman B. Computational thermodynamics. Cambridge: Cambridge University Press; 2007. ISBN 978-0521868112.
[22] Connetable D, Lacaze J, Maugis P, Sundman B. Calphad 2008;32:361–70.
[23] Crystal lattice website. Available from: http://cst-www.nrl.navy.mil/lattice.
[24] Thermo-Calc Software AB, version S. 2008. Available from: http://www.thermocalc.se.
[25] Inden G. Physica 1981;103B:82–100.
[26] Ohnuma I. 2000 [unpublished work].
[27] Kurnakov N, Urasov G, Grigorjew A. Z Anorg Chem 1922;125:207–27.
[28] Gwyer AGC, Phillips HWL. J Inst Met 1927;38:29–83.
[29] Isawa M, Murakamim T. Kinsoku-no-Kenkyu 1927;4:467–77.
[30] Lee JR. J Iron Steel Inst 1960;194:222–4.
[31] Schürmann E, Kaiser H-P. Arch Eisenhuettenwes 1980;51:325–7.
[32] Wachtel E, Bahle J. Z Metallkde 1987;78:229–32.
[33] Wooley F, Elliott JF. Trans AIME 1967;239:1872–83.
[34] Petrushevsky MS, Esin YuO, Gel'd PV, Sandakov VM. Russ Metall 1972;6:149–53.
[35] Dannöhl H-D, Lukas HL. Z Metallkde 1974;65:642–9.
[36] Lee JJ, Sommer F. Z Metallkde 1985;76:750–4.
[37] Mathieu JC, Jounel B, Desré P, Bonnier E. Thermodyn Nucl Mater Symp Vienna 1967; 1968. p. 767–76.
[38] Chipman J, Floridis TP. Acta Metall 1955;3:456–9.
[39] Coscun A, Elliott JF. Trans AIME 1968;242:253–5.
[40] Mitani H, Nagai H. J Jpn Inst Met 1968;32:752–5.
[41] Belton GR, Fruehan RJ. Trans AIME 1969;245:113–7.
[42] Batalin GI, Beloborodova EA, Stukalo VA, Goncharuk LV. Russ J Phys Chem 1971;45:1139–40.
[43] Wever F, Müller A. Z Anorg Allg Chem 1930;192:337–45.
[44] Lesnik AG, Skvorchuk YP. Dopovidi Akad Nauk Ukr RSR 1960:1408–12.
[45] Rocquet P, Jegaden G, Petit JC. J Iron Steel Inst 1967;205:437–41.
[46] Hirano K, Hishinuma A. J Jpn Inst Met 1968;32:516–21.
[47] Rocquet P, Petir JC, Urbain G. J Iron Steel 1971;209:69–70.
[48] Roth A. Z Metallkde 1939;31:299–301.
[49] Crussard C, Aubertin F. Revue Metall 1949;46:661–75.
[50] Edgar JK. Trans AIME 1949;180:225–9.
[51] Nishio M, Nasu S, Murakami Y. J Jpn Inst Met 1970;34:1173–7.
[52] Oscarsson A, Hutchinson WB, Ekström H-E, Dickson DPE, Simensen CJ, Raynaud GM. Z Metallkde 1988;79:600–4.
[53] Sykes C, Evans H. J Iron Steel Inst 1935;131:225–47.
[54] Taylor A, Jones RM. J Phys Chem Solids 1958;6:16–37.
[55] McQueen HJ, Kuczynski GC. Trans AIME 1959;215:619–22.
[56] Lawley A, Cahn RW. J Phys Chem Solids 1961;20:204–21.
[57] Rassmann G, Wich H. Arch Eisenhuettenwes 1962;33:115–22.
[58] Davies RG. J Phys Chem Solids 1963;24:985–92.
[59] Eguchi T, Matsuda H, Oki K, Kioto S-I, Yasutake K. Trans Jpn Inst Met 1967;8:174–9.
[60] Swann PR, Duff WR, Fisher RM. Trans AIME 1969;245:851–3.
[61] Okamoto H, Beck PA. Met Trans 1971;2:569–74.
[62] Köster W, Gödecke T. Z Metallkde 1980;71:765–9.
[63] Fallot M. Ann Phys Paris 1936;6:305–87.
[64] Sucksmith W. Proc R Soc A 1939;170:551–60.
[65] Parsons D, Sucksmith W, Thompson JE. Philos Mag 1958;3:1174–84.
[66] Rimlinger L. C R Acad Sci Paris. 1965;261(Gr.7):4090–3.
[67] Schön CG, Inden G, Eleno LTF. Z Metallkd 2004;95:459–63.
[68] Gonzales-Ormeño PG, Petrilli HM, Schön CG. Scr Mater 2006;54:1271–6.
[69] Gross P, Levi DL, Dewing EW, Wilson GL. Phys Chem Process Metal I Proc Pittsburgh Symp AIME 1959:403–12.
[70] D. Connetable. 2006. [unpublished work].
[71] Dinsdale AT. Calphad 1991;15:317–425.